



**University of
Zurich**^{UZH}

**Zurich Open Repository and
Archive**

University of Zurich
University Library
Strickhofstrasse 39
CH-8057 Zurich
www.zora.uzh.ch

Year: 2017

**Combining ToF-SIMS imaging mass spectrometry and CARS
microspectroscopy reveals lipid patterns reminiscent of gene expression
patterns in the wing imaginal disc of *Drosophila melanogaster***

Marty, Florian ; Rago, Gianluca ; Smith, Donald F ; Gao, Xiaoli ; Eijkel, Gert B ; MacAleese, Luke ;
Bonn, Mischa ; Brunner, Erich ; Basler, Konrad ; Heeren, Ron M A

Abstract: Using label-free ToF-SIMS imaging mass spectrometry, we generated a map of small molecules differentially expressed in the *Drosophila* wing imaginal disc. The distributions of these moieties were in line with gene expression patterns observed during wing imaginal disc development. Combining ToF-SIMS imaging and coherent anti-Stokes Raman spectroscopy (CARS) microspectroscopy allowed us to locally identify acylglycerols as the main constituents of the pattern differentiating the future body wall tissue from the wing blade tissue. The findings presented herein clearly demonstrate that lipids localization patterns are strongly correlated with a developmental gene expression. From this correlation we hypothesize that lipids play a so far unrecognized role in organ development.

DOI: <https://doi.org/10.1021/acs.analchem.7b00125>

Posted at the Zurich Open Repository and Archive, University of Zurich

ZORA URL: <https://doi.org/10.5167/uzh-138706>

Journal Article

Accepted Version

Originally published at:

Marty, Florian; Rago, Gianluca; Smith, Donald F; Gao, Xiaoli; Eijkel, Gert B; MacAleese, Luke; Bonn, Mischa; Brunner, Erich; Basler, Konrad; Heeren, Ron M A (2017). Combining ToF-SIMS imaging mass spectrometry and CARS microspectroscopy reveals lipid patterns reminiscent of gene expression patterns in the wing imaginal disc of *Drosophila melanogaster*. *Analytical Chemistry*, 89(18):9664-9670.

DOI: <https://doi.org/10.1021/acs.analchem.7b00125>

Combining ToF-SIMS imaging mass spectrometry and CARS microspectroscopy reveals lipid patterns reminiscent of gene expression patterns in the wing imaginal disc of *Drosophila melanogaster*

Florian Marty, Gianluca Rago, Donald F. Smith, Xiaoli Gao, Gert B. Eijkel, Luke MacAleese, Mischa Bonn, Erich Brunner, Konrad Basler, and Ron M.A. Heeren

Anal. Chem., **Just Accepted Manuscript** • DOI: 10.1021/acs.analchem.7b00125 • Publication Date (Web): 20 Jul 2017

Downloaded from <http://pubs.acs.org> on August 4, 2017

Just Accepted

"Just Accepted" manuscripts have been peer-reviewed and accepted for publication. They are posted online prior to technical editing, formatting for publication and author proofing. The American Chemical Society provides "Just Accepted" as a free service to the research community to expedite the dissemination of scientific material as soon as possible after acceptance. "Just Accepted" manuscripts appear in full in PDF format accompanied by an HTML abstract. "Just Accepted" manuscripts have been fully peer reviewed, but should not be considered the official version of record. They are accessible to all readers and citable by the Digital Object Identifier (DOI®). "Just Accepted" is an optional service offered to authors. Therefore, the "Just Accepted" Web site may not include all articles that will be published in the journal. After a manuscript is technically edited and formatted, it will be removed from the "Just Accepted" Web site and published as an ASAP article. Note that technical editing may introduce minor changes to the manuscript text and/or graphics which could affect content, and all legal disclaimers and ethical guidelines that apply to the journal pertain. ACS cannot be held responsible for errors or consequences arising from the use of information contained in these "Just Accepted" manuscripts.



Combining ToF-SIMS imaging mass spectrometry and CARS microspectroscopy reveals lipid patterns reminiscent of gene expression patterns in the wing imaginal disc of *Drosophila melanogaster*

Authors: Florian Marty^{1†}, Gianluca Rago^{2,3}, Donald F. Smith², Xiaoli Gao⁴, Gert B. Eijkel^{2,5}, Luke MacAleese^{2††}, Mischa Bonn^{2,3}, Erich Brunner¹, Konrad Basler^{1*}, Ron M.A. Heeren^{2,5*}

Affiliations:

¹Institute of Molecular Life Sciences, University of Zürich, Winterthurerstrasse 190, CH-8057 Zürich, Switzerland

²FOM-Institute AMOLF, Science Park 104, 1098 XG Amsterdam, The Netherlands

³Max Planck Institute for Polymer Research, Ackermannweg 10, 55128 Mainz, Germany

⁴Institutional Mass Spectrometry Laboratory, The University of Texas Health Science Center at San Antonio, 8403 Floyd Curl Drive, MC-7760 San Antonio, TX, USA

⁵The Maastricht Multimodal Molecular Imaging Institute, Maastricht University, Universiteitssingel 50, 6229 ER Maastricht, The Netherlands

*Correspondence to: r.heeren@maastrichtuniversity.nl, konrad.basler@imls.uzh.ch

Current address:

† Biognosys AG, Wagistrasse 21, 8952 Schlieren

†† Groupe de Spectrométries des Biomolécules et Agrégats
Institut Lumière Matière
Cité Lyonnaise de l'Environnement et de l'Analyse
5 rue de la Doua, 69100 Villeurbanne, France

Abstract:

Using label-free ToF-SIMS imaging mass spectrometry, we generated a map of small molecules differentially expressed in the *Drosophila* wing imaginal disc. The distributions of these moieties were in line with gene expression patterns observed during wing imaginal disc development. Combining ToF-SIMS imaging and coherent anti-Stokes Raman spectroscopy (CARS) microspectroscopy allowed us to locally identify acylglycerols as the main constituents of the pattern differentiating the future body wall tissue from the wing blade tissue. The findings presented herein clearly demonstrate that lipids localization patterns are strongly correlated with a developmental gene expression. From this correlation we hypothesize that lipids play a so far unrecognized role in organ development.

One Sentence Summary:

Spatially confined acylglycerols on the surface of the *Drosophila* wing imaginal disc reveal known gene expression patterns important for proper development.

1 Introduction

Tissue and organ development is governed by a multitude of signaling processes, patterning- and growth events. Model organisms such as *Drosophila melanogaster* are often used to study these developmental events and gain fundamental insight of organ development. The majority of pathways governing the development of *Drosophila* are evolutionarily conserved[1]. Therefore, knowledge gained by studying this model organism's development can be transferred to other species such as humans.

The appendages of the adult fly such as wings, legs or antenna develop from organ primordia called imaginal discs[2, 3]. The discs are subdivided into different compartments (e.g. dorsal, ventral, anterior, posterior compartments). The compartments are made of cells with distinct identities that do not mix[4-6]. Compartmentalization is established in the early embryo, when the major body-axes are determined. The compartment boundaries act as organizing centers that govern growth, patterning and development of these discs. The boundaries define the expression of so-called morphogens, proteins which act either locally or diffuse over short and/or long ranges to pattern the growing organ[7-11]. The identification of the molecules (classically proteins and RNAs) are often assigned to defined developmental processes due to their expression patterns or localizations to specific areas of the developing tissue. Genes with similar restricted expression patterns are thought to play related roles. In contrast to the wealth of knowledge that has been obtained about the spatio-temporal restriction of gene expression, as well as that of the corresponding RNAs and proteoforms, the organization and distribution of other molecules, such as carbohydrates and lipids, is not well understood. This lack of knowledge can be traced back to the challenges associated with studying the localization of small molecules, e.g. lipids, with high spatial resolution. Recent work in the model system *Drosophila melanogaster* have described and quantified lipids over the course of its life cycle [12, 13]. These studies demonstrated that different tissues exhibit distinct phospholipid compositions but did not report the intra-organ distribution of these small molecules. Such spatial information is crucial to relate specific molecular moieties to specific biological processes in genetic, disease or developmental models. In order to identify novel small molecules, such as lipids and carbohydrates, that are crucial for a developmental process, we need to look for distribution patterns that resembled those of already known components.

In this work, we determined the distribution of small molecules in the *Drosophila* wing imaginal disc, using a combination of imaging time-of-flight secondary ion mass

spectrometry (ToF-SIMS) and coherent anti-Stokes Raman spectroscopy (CARS). These two complementary, label-free techniques make use of two inherent properties of small molecules, their mass and vibrational properties. We demonstrate that small molecules show well-defined distributions within this tissue. Strikingly, these distributions mimic genetically established patterns known to be essential for wing development and growth.

Material and Methods

Sample preparation

Drosophila melanogaster were grown under standard growth conditions at 22°C. Adult flies were transferred to new food every two days. Wing imaginal discs were manually dissected from wild-type yellow white (*yw*) third instar larvae (day 6 after egg laying) for CARS and ToF-SIMS analyses unless stated otherwise. For ToF-SIMS analysis (results shown in Figures 1A and 2A, B, C), genetically modified *Drosophila* lines with the genotype *yw,hsp-flp; UAS-mCD8::GFP/CyO; hh-Gal4/TM6b* were used³². The *mCD8::GFP* is a fusion protein between mouse lymphocyte marker CD8 and the green fluorescence protein which is expressed under *hh* control in this study. Wing imaginal discs were manually dissected in ice-cold phosphate-buffered saline (PBS) and dehydrated in a 10 × PBS solution (Sigma-Aldrich, Zwijndrecht, NL) for 30 min. For CARS, the discs were then mounted on conventional microscopy cover slides, washed with MS-grade water (Sigma-Aldrich, Zwijndrecht, NL) three times to remove additional salts and then analyzed. For ToF-SIMS, discs were transferred to a conductive ITO slides with 4–8 Ω resistance, Delta Technologies, Stillwater, MN). The discs were washed with MS grade water (Sigma-Aldrich, Zwijndrecht, NL) three times to remove additional salts and then air dried. The discs were then covered with a 2-nm gold layer using a sputter coater (Quorums Technologies SC7640, Newhaven, UK) equipped with a FT7607 quartz crystal microbalance stage and a FT7690 film thickness monitor. For LCMS/MS analysis a Bligh and Dyer extract was prepared from the wingdiscs prior to analysis [14].

Microscopy

Discs were imaged with a Leica DMRX (Leica, Wetzlar, Germany) microscope equipped with an OSRAM HBO 50W/L2 short arc mercury lamp (Osram AG, München, Germany) at 10× magnification.

Data acquisition

ToF-SIMS:

Secondary Ion Mass Spectrometry was performed using a Physical Electronics (PHI) TRIple focusing ToF ion (TRIFT-II) instrument equipped with a gold liquid metal ion gun (Physical Electronics, Chanhassan, MN, USA). Twenty-two keV Au⁺ primary ions were “micro” focused on the sample surface. The total primary ion dose density amount was kept well below the static limit. Positive or negative secondary ions were extracted to the mass analyzer with a static voltage of ±3.5 kV and post-accelerated in front of the ion detector (dual-stage microchannel plate) by an additional 10 kV. Signal from ions in the *m/z* range 1–1500 *m/z* was recorded. Full wing discs were imaged step-by-step in a mosaic formed by 8 × 8 individual tiles between which the stage moved [15, 16]. Each tile of about 80–95 μm in width was probed by the primary ion beam in a 256 × 256 pixel raster for a duration of 30 sec to ensure that the total ion dose was below the static limit of SIMS. The size of each pixel was approximately 0.35 μm. The resulting image was saved as a RAW file for further data processing. The pulse width of the primary ion beam was 1 ns.

CARS microspectroscopy:

A dual-output laser source (Leukos-CARS, Leukos, Limoges, France) provided the pump and Stokes beams to enable CARS analysis. The laser source was a passively Q-switched 1064-nm microchip laser, delivering <1-ns pulses at 32 kHz repetition rate and ~300 mW average power. The laser beam was equally divided into two separate beams with a 50/50 beam splitter. One beam was sent through a bandpass filter (FL1064-10, Thorlabs, USA) and used directly as the pump beam. The other beam was introduced into a photonic crystal fiber that creates super continuum emission of 420–2400 nm at the fiber output, with >100 μW nm⁻¹ spectral power density from 1.05 μm to 1.6 μm. The supercontinuum was coupled out of the fiber with a reflective collimator (RC04APC-P01, Thorlabs, USA) and passed through 700-nm (FEL0700, Thorlabs, USA) and 830-nm (LP02-830RS-25, Semrock, USA) long-pass filters. The Stokes and pump beams overlapped at a dichroic mirror (LP02-1064RU-25, Semrock, USA) and introduced into a modified inverted microscope (Eclipse Ti-U, Nikon, Japan). The pump and Stokes pulses were tightly focused onto the sample with a near IR

1 objective (PE IR Plan Apo 100X, NA 0.75, Seiwa, Japan). The sample was mounted on
2 nested stepper-motor-driven (Microstage, Mad City Labs, USA) and piezo-driven stages
3 (Nano-PDQ 375 HS, Mad City Labs, USA) that together provide 25-mm travel range with
4 <1-nm resolution. The CARS signal generated by the sample was collected in the forward
5 direction by another objective (M-20X, NA 0.4, Newport, USA) and sent through notch
6 (NF03-532/1064E-25, Semrock), USA and short-pass filters (FES1000, Thorlabs, USA) to
7 remove the pump and Stokes beams. The filtered CARS beam was dispersed by a
8 spectrometer (Shamrock 303i, 300 lines mm⁻¹, 1000-nm blaze, Andor, UK) and detected on a
9 deep-depletion CCD (Newton DU920P-BR-DD, Andor, UK). The sample was raster-scanned
10 across the focal volume with steps of 1 μm in-plane and 2 μm axially. Large three-
11 dimensional images were reconstructed from adjacent tiles with in-plane dimensions of 75 ×
12 75 μm or 50 × 50 μm and axial dimension determined by the thickness of the wing disc due
13 to the large dimension of the wing disc. For each position in the sample, a CARS spectrum in
14 the range between -3400 and -600 cm⁻¹ was acquired. CARS images were acquired with pixel
15 dwell times of 50 ms.

16

17 Lipid analysis by HPLC-ESI-MS/MS

18

1
2
3
4
5
6
7
8
9
10
11
12
13
14
15
16
17
18
19
20
21
22
23
24
25
26
27
28
29
30
31
32
33
34
35
36
37
38
39
40
41
42
43
44
45
46
47
48
49
50
51
52
53
54
55
56
57
58
59
60

1 Third instar wing imaginal discs were collected using the mass isolation approach developed
2 in-house as described in [16]. Approximately 1000 individual discs were used per replicate.
3 Lipids were extracted using a modified Bligh and Dyer method [14]. The extracts were
4 removed, dried *in vacuo* and reconstituted in isopropanol. HPLC-ESI-MS/MS analyses were
5 conducted on a Thermo Fisher Q Exactive mass spectrometer (San Jose, CA) with on-line
6 separation using a Thermo Fisher/Dionex RSLC nano HPLC. HPLC conditions were:
7 Atlantis dC18, 3 μm , 300- μm \times 150-mm column (Waters Corporation, Massachusetts);
8 mobile phase A, acetonitrile/water (40:60) containing 10 mM ammonium acetate; mobile
9 phase B, acetonitrile/isopropanol (10:90) containing 10 mM ammonium acetate; flow rate, 6
10 $\mu\text{l}/\text{min}$; gradient, 10% B to 60% B over 5 min, 60% B to 99% B over 35 min and held at 99%
11 B for 10 min. Data-dependent MS/MS scans were performed using one full MS scan [m/z
12 200–2000; 70,000 resolution (m/z 300)] followed by fragmentation in the HCD collision cell
13 of the six most abundant ions in the precursor scan using a normalized collision energy of 35
14 arbitrary units and mass analysis in the Orbitrap at 17,500 resolution. Separate analyses were
15 conducted using positive and negative ions detections.

16
17
18 Data analysis details for all experimental techniques have been provided in the supplemental
19 information.

Results:

Third instar wing imaginal discs were analyzed with ToF-SIMS imaging mass spectrometry in both negative and positive ion mode. Principal component analysis (PCA) was used to unravel the complexity of the ToF-SIMS datasets. Inspection of the principal components (PC) from the negative ion mode measurements revealed four PCs reflecting molecular distributions (**Figure 1**, top row), which co-localized with known genetically predicted tissue sub types such as anterior vs. posterior compartmentalization (A/P) (**Fig. 1A**) and dorsal from ventral tissue (D/V) (**Fig. 1B**). Additionally, patterns reminiscent of the pouch/non-pouch (**Fig. 1C**) and the body wall/wing blade (B/W) (**Fig. 1D**) differentiation were observed. All these compartments are known to play an important role in *Drosophila melanogaster* wing development and are associated with specific gene expression patterns [6, 9, 17-21]. Positive ion mode experiments repeatedly confirmed the B/W distribution and it was therefore chosen to follow up (**Fig. 1E** and **Suppl. Fig.1**).

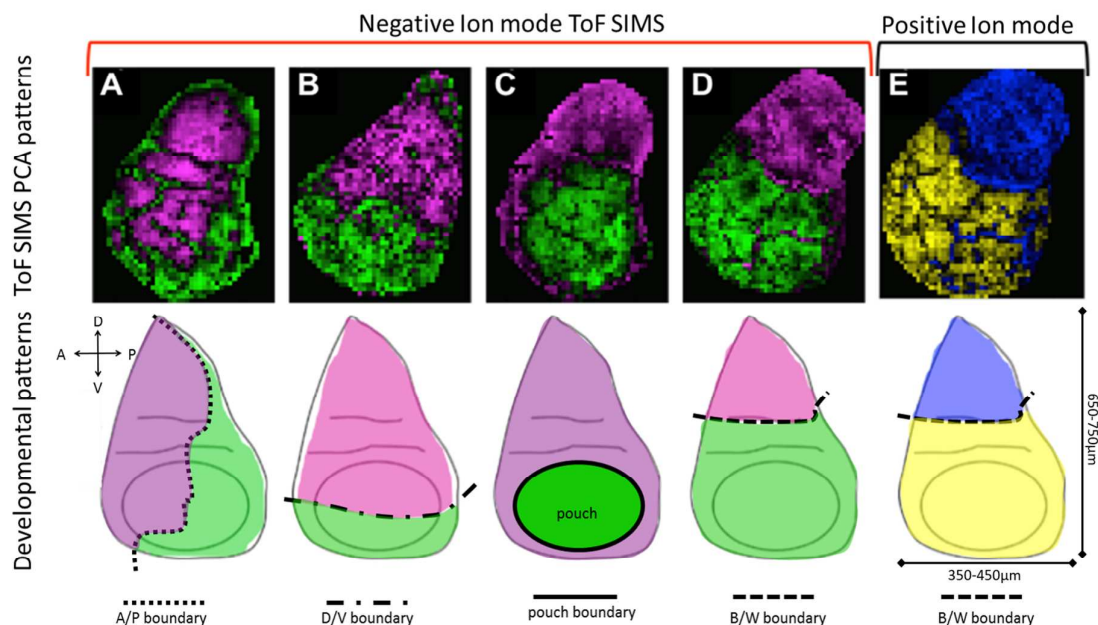


Fig. 1. Small molecule distributions revealed by ToF-SIMS on the wing imaginal disc of *Drosophila melanogaster* (top) and corresponding developmental patterns (bottom (References[22, 23]). PCA of ToF-SIMS PCA data (top row) revealed patterns reminiscent of developmental patterns (bottom row). The patterns anterior/posterior (A/P) (**Fig. 1A**), dorsal/ventral (D/V) (**Fig.1B**), pouch/non-pouch (N/NP) (**Fig.1C**) and body wall/wing blade (B/W) (**Fig.1D**) were detected. The A/P, D/V and P/NP compartments were only observed in negative ion mode. The B/W subdivision was observed in both negative and positive ion modes (**Fig.1E**). A=anterior, P=posterior, D=dorsal, V=ventral, B=body wall, W=wing blade. Wing imaginal discs dimensions indicated.

Next, we determined whether two compartment boundaries (A/P and B/W) observed by ToF-SIMS matched with known developmental boundary markers. For the A/P subdivision, we used the classical compartment boundary established by differential expression of the morphogen *hedgehog* (*hh*), which is responsible for the establishment and maintenance of the A/P compartment [24]. Fluorescent images of third instar imaginal discs expressing GFP under the control of *hh-Gal4* promotor were generated and co-registered with the ToF-SIMS PCA obtained from the same imaginal discs (**Fig. 2A and B**). Clearly, the subdivisions identified by ToF-SIMS were related to the compartmentalization established by the known genetic circuits (**Fig. 2C**).

The B/W compartment boundary (**Fig. 2D**, arrows) is normally delineated by a tissue fold appearing in late third instar[20]. Comparing the total ion image with the PCA image of the same imaginal disc, the fold leading to a crack in the ToF SIMS instrument provides a landmark to determine the expression pattern of small molecules observed by ToF-SIMS in the PCA (**Fig. 2E and F**).

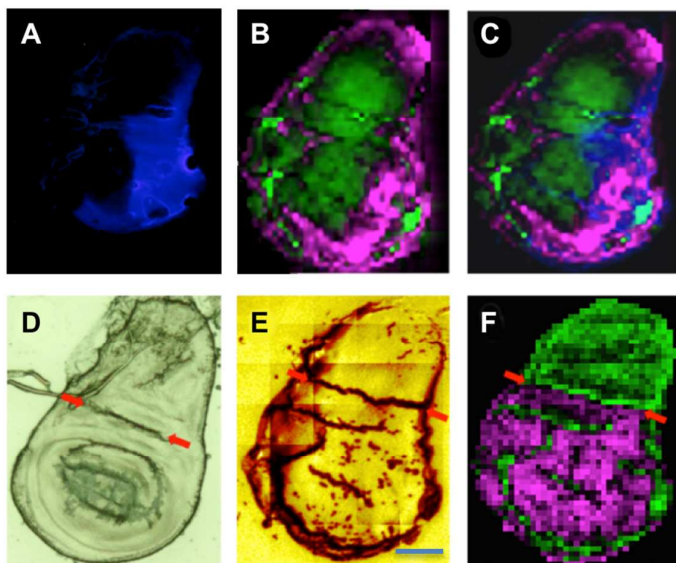


Fig. 2. Small molecule patterns identified by ToF-SIMS mimic known developmental patterns. *Upper panel:* Imaginal disc microscopy images of GFP-labeled *hedgehog* expression patterns that occur exclusively in the posterior compartment (**A**) and ToF-SIMS PCA showing the anterior compartment (green) and posterior compartment (purple)(**B**) of the same imaginal disc were superimposed (**C**). *Lower panel:* The fold appearing in late third instar (**D**, **E**, **F**, red arrows) was used as a landmark for the non-classical body wall/wing blade (B/W) pattern. In the high vacuum of the instrument, this fold expands to a crack (**E**, red arrows). The expression of small molecules, determined by ToF-SIMS PCA, changes exactly at this crack boundary (**F**, red arrows). Thus, both boundaries revealed by PCA coincide with established compartment boundaries in *Drosophila* development. The scale bar in **E** indicates 150 micrometer.

1
2
3 1
4
5 2 The analytical limitation of ToF-SIMS restrict the molecular identification of the PC patterns
6 3 to small molecules [25]. We employed CARS to identify the main small molecule classes
7 4 represented in the ToF-SIMS PCA expression patterns. CARS has the chemical specificity to
8 5 allow the assignment of molecular classes. In that respect the CARS data allows us to
9 6 determine the nature of majority of peaks and provided guidance in the selection of the
10 7 patterns to investigate further. CARS provides image contrast based on molecular vibrations
11 8 that are distinct for different molecules. Using CARS, we acquired the vibrational signatures
12 9 of the molecules (in the frequency range corresponding to Raman shifts from -3200 cm^{-1} to $-$
13 10 900 cm^{-1}) from late third instar wing imaginal discs. In the fingerprinting region (-1800 cm^{-1}
14 11 to -900 cm^{-1}), the chemical moieties giving rise to specific peaks is largely known and can be
15 12 found in the literature [26]. Multivariate statistical analysis (PCA) was applied to screen for
16 13 patterns in the CARS dataset, similar to that performed for the ToF-SIMS datasets. A clear
17 14 B/W pattern similar to the one found by ToF-SIMS (**Fig. 3A, B and C**) is observed. No other
18 15 CARS PCA pattern was observed that resembled any of the previously described patterns.
19 16 Canonical correlation analysis (CCA) revealed a positive correlation score between the
20 17 CARS and ToF-SIMS datasets for the B/W patterns (**Fig. 3C and Supplementary Table 1**).
21 18 Next, we investigated the spectral region of the CARS measurement from the correlating
22 19 value 2 (CV2) to further identify the molecular components of the B/W pattern. In the CARS
23 20 spectra, the dispersive C-H feature and the phenylalanine peak at -1000 cm^{-1} suggested a
24 21 protein dominance for the body wall, whereas the spectral composition indicated a
25 22 dominance of lipids in the wing blade section (**Fig. 3 D**). Therefore, we conclude that the
26 23 components of the B/W patterns observed in ToF-SIMS are lipids. From the ToF-SIMS
27 24 spectra of the wing blade section, we observed a highly reproducible pattern of peaks. Based
28 25 on previously assigned m/z values, 22 lipids were assigned to the classes of monoacyl-
29 26 (MAGs), diacyl- (DAGs) and triacylglycerols (TAGs) (**Fig. 4**) with DAG(34:2/ $375.3m/z$)
30 27 being the most abundant peak in the positive part of the PC loadings spectra. The principal
31 28 component loading spectra show little correlation between the mono- and di-acylglycerols
32 29 and the intact phospholipids. This indicates that these peak most likely do not originate from
33 30 SIMS induced lipid fragmentation. The correlation of the MAG's and DAG's with the TAG's
34 31 indicates that the acylglycerols in general play an important role in maintaining cellular
35 32 organization in the wing discs. Supporting this identification is the observation of the
36 33 corresponding $[M+NH_4]^+$ DAG ions in the LC-MS/MS experiment is an indication that at

least part of the overserved ions are endogenous. However, we cannot exclude that the MAG and DAG related peaks in the SIMS experiments are fragments from TAG's present on the cellular surface. The analysis conditions were optimized to minimize the fragmentation of intact phospholipids and TAG's.

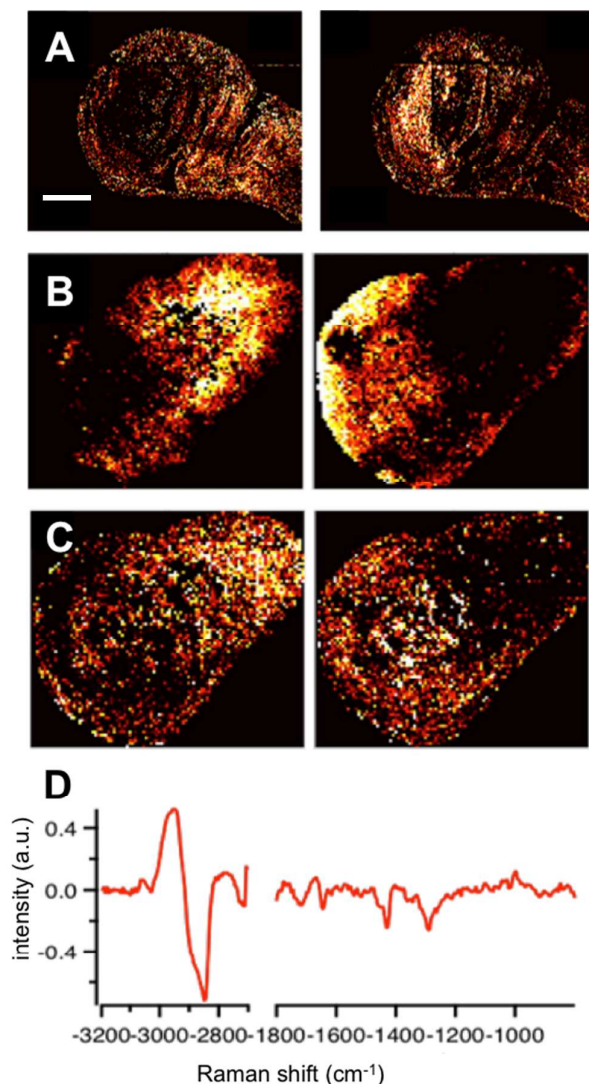


Fig. 3. CARS revealed a lipid origin for the B/W pattern: CARS was applied to test if patterns observed by ToF-SIMS can be reproduced and to gain further knowledge about the molecules involved. PCA of CARS data demonstrated a similar B/W pattern (A) to that observed in ToF-SIMS (B). CCA was applied to visualize the correlation of the observed patterns from ToF-SIMS and CARS (C; quantification listed in **Supplementary Table 1**). Investigation of the normalized CARS spectra in arbitrary units (a.u.) revealed a higher content of lipids in the wing blade region compared to the body wall (D). The scale bar in A indicates 200 micrometer. The left and right images in all panels A-D represent principal components in the 3200-2700 cm⁻¹ and the 1800-800 cm⁻¹ wavenumber range respectively.

To confirm this identification of the ToF-SIMS peaks, we performed orthogonal validation using high-performance liquid chromatography, electrospray ionization tandem mass spectrometry (HPLC-ESI-MS/MS, hereafter referred to as MS/MS for simplicity) of lipid extracts of whole wing imaginal disc [27]. This dataset was utilized as a high-mass-accuracy MS reference data set for tissue-specific lipids. We identified 156 lipid species (for details, see *Materials and Methods* section) containing most of the major lipid classes previously assigned [12, 13]. Of the 156 lipid species, 5 were MAGs, 22 DAGs and 10 TAGs. Seven species overlapped between the differential patterns observed by ToF-SIMS and MS/MS methods (**Table 1**). Among these lipids was also the previously reported DAG(34:2). Its identity in the ToF-SIMS data could further be confirmed using the loadings spectra from the negative ion mode ToF-SIMS data (**Suppl. Fig 2**).

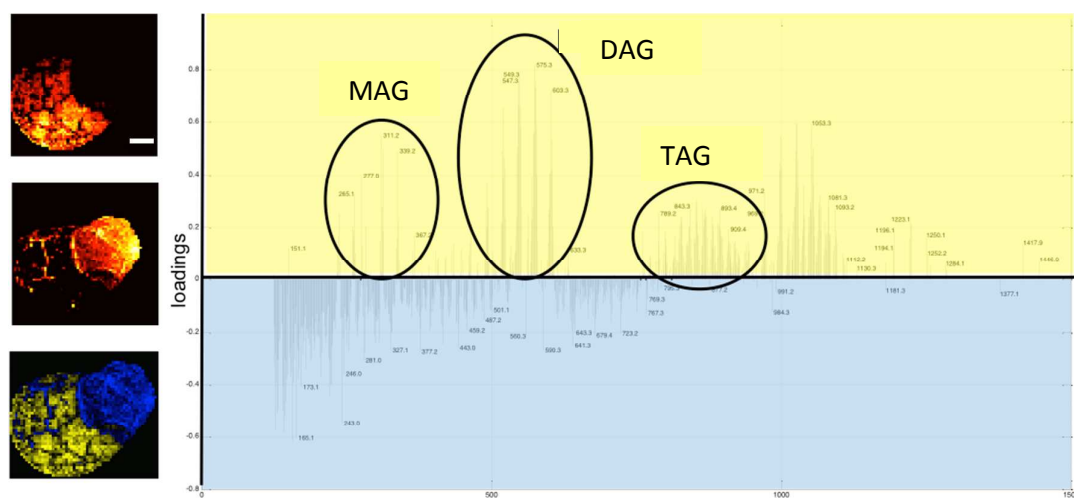


Fig. 4. Assignment of peaks from ToF-SIMS measurements: The images shows the positive and negative part of the PC distinguishing the B/W compartments (left top and middle panel) from the same imaginal disc as used in Figure 1. The loading spectrum on the right shows the positive loadings corresponding to W with a yellow background and negative loadings corresponding to B with a lightblue background. The lower left panel is a color coded overlay (yellow=W, blue=B). To assign the potential lipid species, we used a recently published m/z catalogue with assigned lipids [12]. Loading spectra show that monoacyl- (MAG), diacyl- (DAG) and triacylglycerols (TAG) are overrepresented in the wing blade section (yellow). The white scale bar in the top left image indicates 150 micrometer.

Lipid class (C:DB)	Passarelli et al. m/z	Adduct	ToF-SIMS						LC MS/MS m/z	Adduct	Monoisotopic mass	
			Rep. 1 m/z	Rep. 2 m/z	Rep. 3 m/z	Rep. 4 m/z	Rep. 5 m/z	Rep. 6 m/z				
MAG(16:1)	311.3	[M+H-H ₂ O] ⁺	311.2	311.1	311.1	311.1	311.1	311.1	n.d.	-	328.2614	
MAG(16:0)	313.3	[M+H-H ₂ O] ⁺	313.2	313.1	313.1	n.d.	n.d.	313.1	348.3092	[M+NH ₄] ⁺	330.2270	
MAG(18:1)	339.3	[M+H-H ₂ O] ⁺	339.2	339.2	339.2	339.2	339.2	339.2	n.d.	-	356.2927	
DAG(30:2)	519	[M+H-H ₂ O] ⁺	519.3	519.3	519.3	519.3	519.3	519.3	n.d.	-	536.4441	
DAG(30:1)	521	[M+H-H ₂ O] ⁺	521.3	521.3	521.2	521.3	521.2	521.2	n.d.	-	538.4597	
DAG(30:0)	523	[M+H-H ₂ O] ⁺	523.3	523.3	523.3	523.3	523.3	523.3	n.d.	-	540.4754	
DAG(32:2)	547	[M+H-H ₂ O] ⁺	547.3	547.3	547.2	547.3	547.2	547.2	n.d.	-	564.4754	
DAG(32:1)	549	[M+H-H ₂ O] ⁺	575.3	575.3	575.3	575.3	575.3	575.3	567.4964	[M+H] ⁺	566.4910	
DAG(32:0)	551	[M+H-H ₂ O] ⁺	551.3	551.3	551.3	551.3	551.3	551.3	586.5389	[M+NH ₄] ⁺	568.5067	
DAG(34:3)	573	[M+H-H ₂ O] ⁺	573.3	573.3	573.2	573.3	573.3	573.2	608.5209	[M+NH ₄] ⁺	590.4910	*
DAG(34:2)	575	[M+H-H ₂ O] ⁺	575.3	575.3	575.3	575.3	575.3	575.3	593.5110	[M+H] ⁺	592.5067	
DAG(34:1)	577	[M+H-H ₂ O] ⁺	577.3	577.3	577.3	577.3	577.3	577.3	612.5544	[M+NH ₄] ⁺	594.5223	
DAG(34:0)	579	[M+H-H ₂ O] ⁺	579.3	579.3	579.2	n.d.	n.d.	579.2	n.d.	-	596.5380	
DAG(36:4)	599	[M+H-H ₂ O] ⁺	599.3	599.2	599.2	599.2	599.2	599.2	634.5365	[M+NH ₄] ⁺	616.5067	*
DAG(36:3)	601	[M+H-H ₂ O] ⁺	601.3	601.3	601.2	601.2	601.2	601.2	n.d.	-	618.5223	*
DAG(36:2)	603	[M+H-H ₂ O] ⁺	603.3	603.3	603.3	603.3	603.3	603.2	n.d.	-	620.5380	
TAG(50:3)	851	[M+Na] ⁺	n.d.	n.d.	n.d.	n.d.	851.3	n.d.	n.d.	-	828.7207	
TAG(50:2)	853	[M+Na] ⁺	853.4	n.d.	853.3	853.3	853.3	853.3	n.d.	-	830.7363	
TAG(50:1)	855	[M+Na] ⁺	855.4	n.d.	n.d.	n.d.	855.3	n.d.	n.d.	-	832.7520	
TAG(52:3)	879	[M+Na] ⁺	n.d.	n.d.	n.d.	n.d.	879.3	n.d.	n.d.	-	856.7520	
TAG(52:2)	881	[M+Na] ⁺	n.d.	n.d.	n.d.	n.d.	881.3	n.d.	n.d.	-	858.7676	
TAG(52:1)	883	[M+Na] ⁺	n.d.	n.d.	n.d.	883.3	n.d.	n.d.	n.d.	-	860.7833	

Table 1. Identified MAGs, DAGs, and TAGs by ToF-SIMS and MS/MS: The columns show the lipid class, mass value (*m/z*), species as well as the monoisotopic mass of each lipid identified in the six replicate ToF-SIMS measurements (Fig. S1). The lipids identified by both ToF-SIMS and MS/MS are highlighted in yellow. The most abundant peak of the ToF-SIMS loading spectra (*m/z* 573.3) also identified by MS/MS is shown in blue text. n.d indicates a non-detected species in that measurement. The asterix in the last column indicates that the listed SIMS *m/z* values could also be explained as the sodium adduct of an ion that contains 2 carbon atoms and 3 double bonds less. For example [M+H-H₂O]DAG36:4 is nominally equivalent with [M+Na-H₂O]DAG34:1.

Discussion

In this study, we applied ToF-SIMS to analyze the distribution of small molecules in the wing imaginal disc of third instar *Drosophila melanogaster* larvae. We found that their distributions separated into two PCs with distinct subdivisions (Fig. 1). Intrigued by these ToF-SIMS patterns, we compared them to known genetic expression patterns at the same developmental time-point and found striking similarities. These pattern similarities were in part confirmed by co-registration of images of GFP fluorescence under *hedgehog* promotor control, a classical marker of the A/P compartment boundary. Additionally the B/W pattern is defined and confirmed by a well-known visible margin that correlates with the ToF-SIMS images (Fig. 2). By investigating CARS PCA spectra (Fig. 3) and tentative assignments from ToF-SIMS peaks (Fig. 4), using a previously published catalogue, we identified the predominant small molecules species in the wing blade region of the B/W pattern as lipids.

1 The possible role of these lipids in pattern formation and maintenance must be evaluated in
2 light of their crucial metabolic and biochemical properties. Recent lipidomic studies revealed
3 that DAGs and TAGs levels increase in the wing imaginal disc during larval development,
4 reaching a peak at late third instar [12, 13]. While TAGs are mainly considered storage lipids
5 from which energy can be gained via β -oxidation [28, 29], they are not used for energy
6 production during pupation and metamorphosis [12]. Whether TAGs assume a different
7 function in imaginal discs remains to be elucidated. In contrast to TAGs, DAGs show
8 different kinetics based on their fatty acid (FA) chain length. Medium-FA-chain DAGs
9 drastically decrease at the transition from third larval instar to the pupa stage whereas long-
10 chain DAGs continue to increase, which suggests that different DAGs assume distinct
11 metabolic functions during *Drosophila* development; these functions also remain to be
12 determined. We identified one DAG, termed DAG(34:2), by both ToF-SIMS and MS/MS,
13 and found intermediate chain C16:1 and C18:1 as the two most abundant FA in this DAG.
14 This, and other intermediate-chain DAGs, may be used as building blocks for the rapid
15 synthesis of new phospholipids.

16 Several roles of DAGs have been described. Some DAGs serve as second messengers in
17 several receptor signal transductions via the hydrolysis of membrane lipids into DAGs and
18 inositol-3,4,5-triphosphate (IP₃) by the enzyme phospholipase C. The generation of IP₃ leads
19 to a release of Ca²⁺ from the endoplasmic reticulum. Ca²⁺ together with the DAG signaling
20 pathway governs processes like cell division and differentiation [30]. Additionally,
21 phospholipase D activity is known to regulate cell growth and proliferation using Raf and
22 mTOR as mediators [31]. DAGs remodel the membrane in response to effector signals,
23 which might contribute to compartment boundary formation and maintenance. In the immune
24 system, for example, successful phagocytosis requires actin remodeling by DAG generation
25 [32]. Other mechanisms leading to similar membrane remodeling and polarization are
26 reviewed in [33]. It has been demonstrated elsewhere that DAGs in combination with other
27 membrane lipids in distinct proportions have an important function in determining the
28 structure and dynamics of biological membranes [34]. For example, the membrane
29 composition of a cell is important for the curvature of the membrane itself on a single cell
30 level [35]. Likewise, it can be presumed that the membrane composition of a sub-tissue
31 region, such as a compartment, may influence the curvature of the tissue. Such a phenomenon
32 might be responsible for the generation of tissue folds, and our data seem to be consistent
33 with this notion (**Figs. 1 and 2**). Alternatively, an overrepresentation of DAGs in one cell

1
2
3
4
5
6
7
8
9
10
11
12
13
14
15
16
17
18
19
20
21
22
23
24
25
26
27
28
29
30
31
32
33
34
35
36
37
38
39
40
41
42
43
44
45
46
47
48
49
50
51
52
53
54
55
56
57
58
59
60

1 population might increase the cells' affinity to each other and thereby contribute to the
2 segregation of cells of different populations. We hypothesize that DAGs might also be
3 differentially distributed in the two leaflets of the lipid bilayer as a consequence of the
4 increasing tension generated during metamorphosis. As the organism undergoes tremendous
5 change during pupariation, it is likely that an enormous amount of membranes must be
6 generated in a very short time. The lipid patterns observed from our studies offer important
7 insights for the potential role(s) of lipids during *Drosophila* wing development and cellular
8 organization.
9

1

Acknowledgments: This project was financed in part with a grant from the Swiss SystemsX.ch initiative, grant IPP-2011/“Identification of Small Molecules Relevant for Patterning and Growth of the Wing Imaginal Disc Using High Resolution Mass Spectrometry” to EB, KB and RMAH. This work is part of the research program of the Stichting voor Fundamenteel Onderzoek der Materie (FOM), which is financially supported by the Nederlandse Organisatie voor Wetenschappelijk Onderzoek (NWO). RMAH acknowledges support from the Dutch province of Limburg under the LINK program. We also thank the Kanton of Zürich and the Swiss National Science Foundation for support. Special thanks to Dr. George Hausmann and Dr. Kerstin Euler for critical input on the manuscript, and Robin Klemm for interesting discussions.

12

13 References:

14

- 15 1. French, V., Bryant, P.J., Bryant, S.V.: Pattern Regulation in Epimorphic Fields. *Science*. **193**, 969-981 (1976)
- 16 2. Fristrom, J.W., Mitchell, H.K.: Preparative Isolation of Imaginal Discs from Larvae of *Drosophila Melanogaster*. *J Cell Biol.* **27**, 445 (1965)
- 17 3. Postlethwait, J.H., Schneiderman, H.A.: Pattern Formation in Imaginal Disks of *Drosophila-Melanogaster* after Irradiation of Embryos and Young Larvae. *Dev Biol.* **32**, 345-360 (1973)
- 18 4. Gonzalezgaitan, M., Capdevila, M.P., Garciabellido, A.: Cell-Proliferation Patterns in the Wing Imaginal Disc of *Drosophila*. *Mech Develop.* **46**, 183-200 (1994)
- 19 5. Fraser, S., Keynes, R., Lumsden, A.: Segmentation in the Chick-Embryo Hindbrain Is Defined by Cell Lineage Restrictions. *Nature*. **344**, 431-435 (1990)
- 20 6. Schilling, S., Willecke, M., Aegerter-Wilmsen, T., Cirpka, O.A., Basler, K., von Mering, C.: Cell-Sorting at the A/P Boundary in the *Drosophila* Wing Primordium: A Computational Model to Consolidate Observed Non-Local Effects of Hh Signaling. *Plos Comput Biol.* **7**, (2011)
- 21 7. Zecca, M., Basler, K., Struhl, G.: Direct and long-range action of a wingless morphogen gradient. *Cell*. **87**, 833-844 (1996)
- 22 8. Nellen, D., Burke, R., Struhl, G., Basler, K.: Direct and long-range action of a DPP morphogen gradient. *Cell*. **85**, 357-368 (1996)
- 23 9. Kornberg, T.B., Guha, A.: Understanding morphogen gradients: a problem of dispersion and containment. *Curr Opin Genet Dev.* **17**, 264-271 (2007)
- 24 10. Tabata, T.: Genetics of morphogen gradients. *Nat Rev Genet.* **2**, 620-630 (2001)
- 25 11. Campbell, G., Tomlinson, A.: Transducing the Dpp morphogen gradient in the wing of *Drosophila*: Regulation of Dpp targets by brinker. *Cell*. **96**, 553-562 (1999)

38

1
2
3
4
5
6
7
8
9
10
11
12
13
14
15
16
17
18
19
20
21
22
23
24
25
26
27
28
29
30
31
32
33
34
35
36
37
38
39
40
41
42
43
44
45
46
47
48
49
50
51
52
53
54
55
56
57
58
59
60

12. Guan, X.L., Cestra, G., Shui, G.H., Kuhrs, A., Schittenhelm, R.B., Hafen, E., et al.: Biochemical Membrane Lipidomics during *Drosophila* Development. *Dev Cell*. **24**, 98-111 (2013)

13. Carvalho, M., Sampaio, J.L., Palm, W., Brankatschk, M., Eaton, S., Shevchenko, A.: Effects of diet and development on the *Drosophila* lipidome. *Mol Syst Biol*. **8**, (2012)

14. Bligh, E.G., Dyer, W.J.: A Rapid Method of Total Lipid Extraction and Purification. *Can J Biochem Phys*. **37**, 911-917 (1959)

15. Lee, T., Luo, L.Q.: Mosaic analysis with a repressible cell marker for studies of gene function in neuronal morphogenesis. *Neuron*. **22**, 451-461 (1999)

16. Marty, F., Rockel-Bauer, C., Simigdale, N., Brunner, E., Basler, K.: Large-scale imaginal disc sorting: A protocol for "omics"-approaches. *Methods*. **68**, 260-264 (2014)

17. Zecca, M., Struhl, G.: Control of growth and patterning of the *Drosophila* wing imaginal disc by EGFR-mediated signaling. *Development*. **129**, 1369-1376 (2002)

18. Ng, M., Diazbenjumea, F.J., Cohen, S.M.: Nubbin Encodes a Pou-Domain Protein Required for Proximal-Distal Patterning in the *Drosophila* Wing. *Development*. **121**, 589-599 (1995)

19. Irvine, K.D., Rauskolb, C.: Boundaries in development: Formation and function. *Annu Rev Cell Dev Bi*. **17**, 189-214 (2001)

20. Diez del Corral, R., Aroca, P., Gomez-Skarmeta, J.L., Cavodeassi, F., Modolell, J.: The Iroquois homeodomain proteins are required to specify body wall identity in *Drosophila*. *Gene Dev*. **13**, 1754-1761 (1999)

21. Tabata, T., Kornberg, T.B.: Hedgehog Is a Signaling Protein with a Key Role in Patterning *Drosophila* Imaginal Disks. *Cell*. **76**, 89-102 (1994)

22. True, J.R.: Insect melanism: the molecules matter. *Trends Ecol Evol*. **18**, 640-647 (2003)

23. Dahmann, C., Basler, K.: Compartment boundaries - at the edge of development. *Trends Genet*. **15**, 320-326 (1999)

24. Dahmann, C., Basler, K.: Opposing transcriptional outputs of hedgehog signaling and engrailed control compartmental cell sorting at the *Drosophila* A/P boundary. *Cell*. **100**, 411-422 (2000)

25. Passarelli, M.K., Winograd, N.: Lipid imaging with time-of-flight secondary ion mass spectrometry (ToF-SIMS). *Bba-Mol Cell Biol L*. **1811**, 976-990 (2011)

26. Movasaghi, Z., Rehman, S., Rehman, I.U.: Raman spectroscopy of biological tissues. *Appl Spectrosc Rev*. **42**, 493-541 (2007)

27. Gao, X.L., Zhang, Q.B., Meng, D., Isaac, G., Zhao, R., Fillmore, T.L., et al.: A reversed-phase capillary ultra-performance liquid chromatography-mass spectrometry (UPLC-MS) method for comprehensive top-down/bottom-up lipid profiling. *Anal Bioanal Chem*. **402**, 2923-2933 (2012)

28. Coleman, R.A., Mashek, D.G.: Mammalian Triacylglycerol Metabolism: Synthesis, Lipolysis, and Signaling. *Chem Rev*. **111**, 6359-6386 (2011)

29. Athenstaedt, K., Daum, G.: The life cycle of neutral lipids: synthesis, storage and degradation. *Cell Mol Life Sci*. **63**, 1355-1369 (2006)

30. Harden, T.K., Sondek, J.: Regulation of phospholipase C isozymes by Ras superfamily GTPases. *Annu Rev Pharmacol*. **46**, 355-379 (2006)

31. Hodgkin, M.N., Pettitt, T.R., Martin, A., Michell, R.H., Pemberton, A.J., Wakelam, M.J.O.: Diacylglycerols and phosphatidates: which molecular species are intracellular messengers? *Trends Biochem Sci*. **23**, 200-204 (1998)

- 1
2
3 1 32. Scott, C.C., Dobson, W., Botelho, R.J., Coady-Osberg, N., Chavrier, P., Knecht,
4 2 D.A., et al.: Phosphatidylinositol-4,5-bisphosphate hydrolysis directs actin
5 3 remodeling during phagocytosis. *J Cell Biol.* **169**, 139-149 (2005)
6 4 33. Almena, M., Merida, I.: Shaping up the membrane: diacylglycerol coordinates spatial
7 5 orientation of signaling. *Trends Biochem Sci.* **36**, 593-603 (2011)
8 6 34. Sprong, H., van der Sluijs, P., van Meer, G.: How proteins move lipids and lipids
9 7 move proteins. *Nat Rev Mol Cell Bio.* **2**, 504-513 (2001)
10 8 35. Cooke, I.R., Deserno, M.: Coupling between lipid shape and membrane curvature.
11 9 *Biophys J.* **91**, 487-495 (2006)
12 10
13
14
15
16
17
18
19
20
21
22
23
24
25
26
27
28
29
30
31
32
33
34
35
36
37
38
39
40
41
42
43
44
45
46
47
48
49
50
51
52
53
54
55
56
57
58
59
60